Smart Windows for Building Integration: A New Architecture for Photovoltachromic Devices

Francesco Malara,*,⊥,† Alessandro Cannavale,*,⊥,‡ Sonia Carallo,† and Giuseppe Gigli†,‡,§

†National Nanotechnology Laboratory (NNL), CNR Istituto Nanoscienze, c/o Distretto Tecnologico, Via Arnesano km 5, 73100 Lecce, Italy

‡CBN, Center for Biomolecular Nanotechnologies, Fondazione Istituto Italiano di Tecnologia—Energy Platform, Via Barsanti, 73010 Arnesano (Lecce), Italy

§Dipartimento di Matematica e Fisica "E. De Giorgi"—Università del Salento, via per Arnesano, 73100 Lecce, Italy

ABSTRACT: A new architecture for multifunctional photo-electrochemical devices, namely photovoltachromic devices, is disclosed here, capable of producing electric energy by solar conversion also modulating the devices' optical transmittance in a smart and aesthetically sounding fashion. These devices generally consist of a titanium dioxide photoelectrode and of a bifunctional patterned counter electrode made of platinum and amorphous tungsten oxide. The innovative configuration described hereafter proposes to split the single patterned counter electrode into two distinct electrodes, physically overlapped: the central one is suitably drilled in order to allow the electrolyte to fill both communicating chambers. These three electrode devices allow three independent operating modes: photovoltaic, photoelectrochromic, and photovoltachromic. In this paper, we report the optical, electrical, and electrochemical characterization of this innovative device, varying both available catalytic surface area and the type of sensitizing dye. We eventually obtained the following conversion efficiencies, 2.75%, 2.35%, and 1.91%, in samples having different catalytic areas (397, 360, and 320 mm^2, respectively). We inferred that the higher the platinum area on the interposed platinum—poly(ethylene naphthalate)—indium tin oxide counter electrode, the higher the photovoltaic conversion efficiency. On the other hand, a decrease of the intercommunication openings generates a slowdown of bleaching processes.

KEYWORDS: smart windows, photovoltachromic cells, chromogenics, building integration, dye-sensitized cells
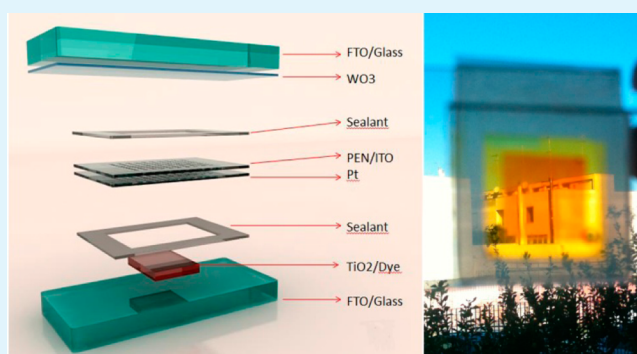
1. INTRODUCTION

In recent years, several research activities have been directed toward smart materials and devices in order to achieve a dynamic solar control in transparent building envelopes. The open issue of building integration of "smart windows" is nowadays crucial, considering that the built environment uses as much as 30−40% of primary energy worldwide. As a matter of fact, a large number of studies are currently dealing with chromogenic devices.[1,2]

It has been demonstrated that electrochromic (EC) and photovoltachromic (PVCC) windows enhance the energy performances of windows with respect to conventional shading and solar control devices. This generates several advantages, such as the reduction of cooling costs, heating, and ventilation loads, as well as a considerable cut in the use of artificial lighting, due to a more correct use of day lighting.[3−6]

A very promising category of "smart" chromogenic devices is represented by photoelectrochromics cells (PECCs), a special kind of self-powered smart windows.[7,8] These are electrochemical cells consisting of two electrodes, separated by a redox electrolyte. The photoanode is coated with a layer of dye-sensitized mesoporous TiO$_2$ (on a transparent conductive

oxide), whereas a cathodic electrochromic material is deposited on the counter electrode (generally WO$_3$).[9,10] So far, several architectures[11−16] have been proposed for these devices, for which the coloration process is self-generated, depending on the available irradiance, and does not require any external voltage.[17−22]

In 2009, Wu et al.[23] developed a novel device, namely a photovoltachromic cell (PVCC), composed of a patterned WO$_3$/Pt electrochromic counter electrode and a dye-sensitized TiO$_2$ photoanode, proving the reliability of an approach integrating dye-sensitized solar cell (DSSC)[24] and photo-electrochromic (PEC) technologies. However, the energy conversion efficiency exhibited by the PVCC was about 0.5%, and it did not allow to manage separately DSSC and PEC functionalities.

Recently, we proposed a complete separation of two areas on the counter electrode, respectively devoted to coloration (WO$_3$) and to photovoltaic conversion (Pt).[25,26] This design
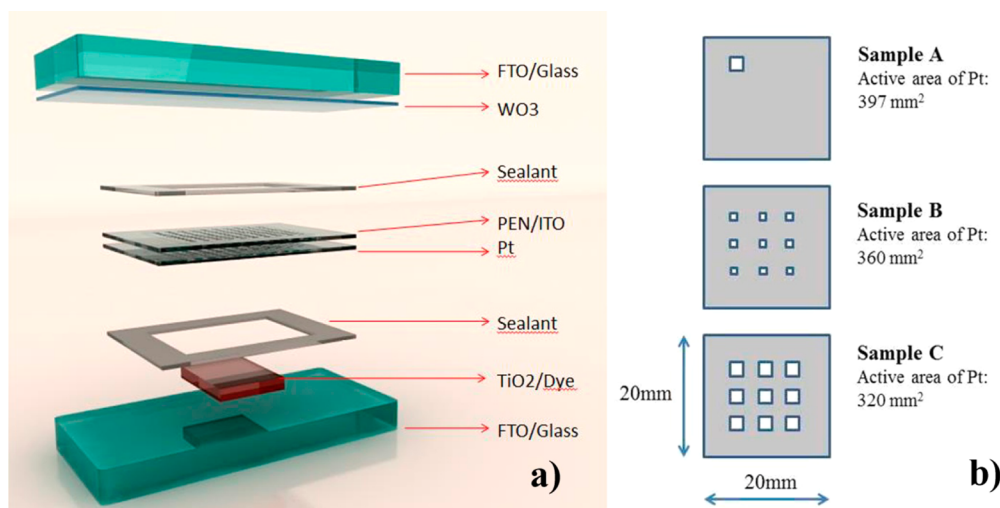
Figure 1. (a) Exploded view of the device. TiO_2 and WO_3 were deposited on FTO/glass substrates, whereas Pt was deposited on PEN/ITO substrate. The latter electrode was drilled allowing the electrolyte to fill the two resulting chambers. The three electrodes are then mutually sealed by Surlyn films. The device was filled with the electrolyte through a predrilled hole made on the WO3 electrode. (b) Schematic representation of three different counter electrodes studied; the white squares represent the openings made on each electrode.

also allowed a bifunctional and interactive management of the device features. Nevertheless the counter electrode, electrically divided into two areas, produced an aesthetically nonoptimized appearance. In fact, only a part of the device was capable of smart coloration, while the remaining part was not involved in the chromic transition, thus resulting as opaque or bleached.

In the present work, we show a completely new architecture for photovoltachromic devices (Figure 1) undergoing smart and homogeneous coloration and bleaching, perfectly suitable for building integration. It is based on three distinct electrodes, assembled as follows: a highly transparent photoelectrode, a very thin Pt electrode deposited on a PEN-ITO substrate, and a WO_3 electrode, superimposed in a "sandwich" configuration. The central platinum electrode was previously drilled in order to permit the creation of a unique electrolytic chamber inside the device. The electrolyte fills the two interspaces generating a suitable electrochemical link. Here, we describe the possible configurations between DSSC, PECC, and PVCC modes and report the electrochemical characterizations carried out in order to demonstrate the effectiveness of such architecture. We investigated the PV properties corresponding to the variation of the Pt area, as a consequence of the different sizes of predrilled holes made on the central electrode. Moreover, an organic dye (DYE1) was adopted, and its beneficial effects on the transmittance of devices were assessed.

2. EXPERIMENTAL SECTION

2.1. Preparation of TiO_2 Nanorods Paste. TiO_2 nanorods were prepared according to a procedure described elsewhere.[27−29] Briefly, in a typical synthesis, titanium tetraisopropoxide (TTIP, 17.7 mL, 60 mmol) was added to 50 g of oleic acid at room temperature. Then, the resulting mixture was gradually heated to 270 °C at a rate of about 10 °C/min and then kept at this temperature for 2 h. After the synthesis, the TiO_2 nanocrystals were precipitated upon addition of ethanol or 2-propanol: acetone mixtures, separated by centrifugation and washed with acetone to remove the excess surfactant residuals. Then, the resulting products were easily redispersed in an apolar organic solvent, such as toluene or chloroform. Nanocrystal suspensions were stirred at 60 °C for 6 h with ethyl cellulose previously dissolved in toluene (10 wt %/wt). The exchanged solvent was carried out as follows: terpineol was added and the resulting mixture was stirred again for 1 h; finally

toluene was removed by a rotary evaporator to obtain pastes suitable for doctor-blade deposition. The paste had the following weight percentage composition: TiO_2: 12%; organic capping residuals: 15%; ethyl cellulose: 5%; terpineol: 68%.

2.2. Preparation of Counter Electrodes. Three different ITO/PEN substrates were prepared to deposit platinum layers by high vacuum electron beam evaporation (TemescalSupersource). Holes having different sizes were drilled on ITO/PEN substrates: 3.14, 40, and 80 mm^2. This resulted in different values of Pt catalytic area: 396.86, 360, and 320 mm^2. For clearness sake, devices embodying such counter electrodes were named, respectively, sample A, sample B, and sample C, respectively.

The vacuum chamber was initially evacuated to 10^{-7} mbar, and then the first 2 nm adhesion layer of titanium was deposited. The platinum coating, having a thickness of 5 nm, was then deposited. The rate of deposition was about 0.5 Å/s, and the e-beam power was about 30%. During the deposition, the vacuum chamber reached a temperature of about 40 °C.

Tungsten oxide layers were deposited by electron beam deposition on ITO/glass substrates. The vacuum chamber was initially evacuated to 10^{-7} mbar, and then pure dry oxygen was admitted through a needle valve (20 sccm). The pressure was maintained at 10^{-4} mbar throughout the process. The deposition rate was about 1.5 Å/s, and the e-beam power was about 8%. During the deposition the chamber reached a temperature of about 210 °C.

2.3. Preparation of Photoelectrodes. FTO glasses were cleaned in a detergent solution using an ultrasonic bath for 15 min and then washed with water and ethanol. The TiO_2 nanorods paste was deposited onto F-doped tin oxide (FTO) conducting glass by doctor blading and gradually heated in an oven at air atmosphere; the temperature gradient program had three levels at 170 °C (40 min), 350 °C (15 min), and 430 °C (30 min). All the films had the same value of active area (1 cm^2) and a thickness of about 5 μm.

The photovoltaic and electrochemical characterizations were performed on TiO_2 electrodes immersed into a solution 0.5 mM of (bis(tetrabutylammonium)-cis-di(thiocyanato)-N,N'-bis(4-carboxyla-to-4'-carboxylic acid-2,2-bipyridine) ruthenium(II) (N719) in a mixture of acetonitrile and tert-butyl alcohol (v/v, 1:1). After a 1 h dye-loading process, the N719 sensitized film exhibited a transparency superior to 25% in the blue-green region and higher than 50% in the red/near-IR region, whereas after 12 h the transmittance in the visible range was almost completely cut down. Since good transparency in the visible range represents a crucial feature for a fully integrated photovoltachromic window, we finally used a 1 h sensitized N719 electrode.
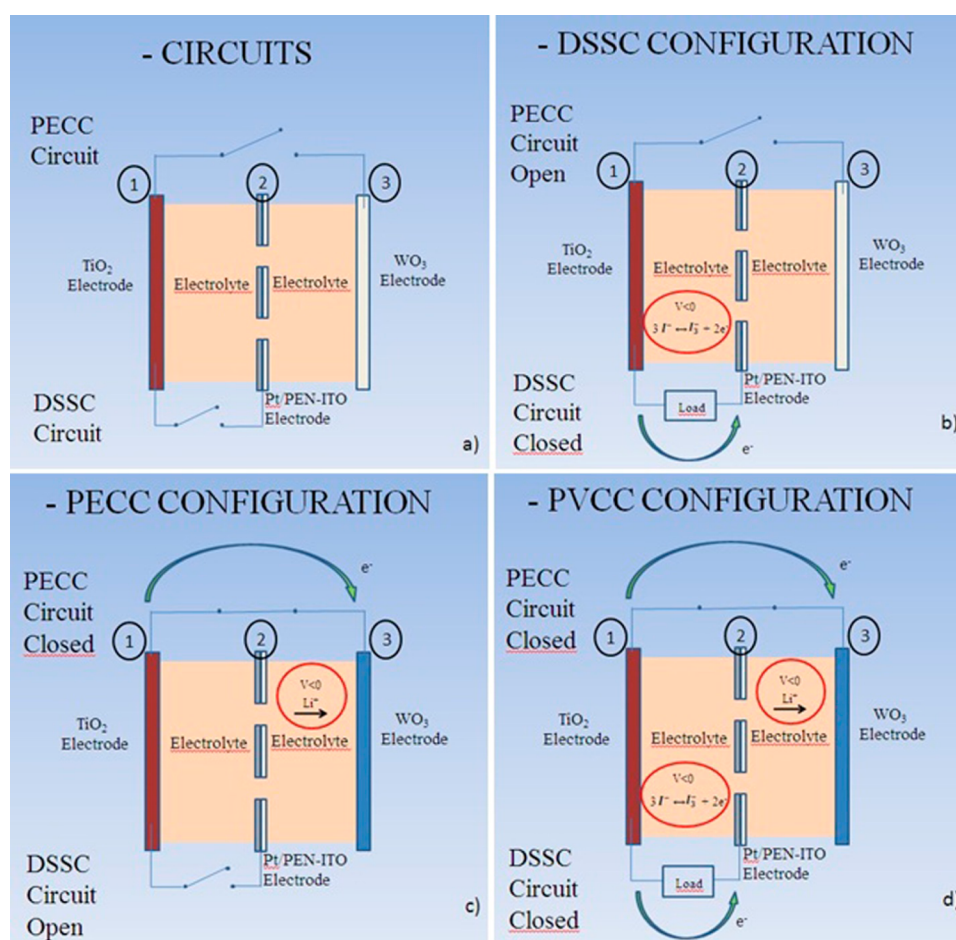
Figure 2. Scheme of the device cross section, representing the operating modes of the three-electrode PVCC device. Three configurations are possible: DSSC, PECC, or PVCC, depending on which circuit is closed. (a) Representation of the device circuits in open condition. (b) DSSC configuration: closed circuit between TiO_2 and Pt-PEN-ITO electrode. (c) PEC configuration: electric connection between TiO_2 and WO_3. (d) PVCC configuration: when both circuits (DSSC and PECC) are closed.

2.4. Fabrication of Photovoltachromic Devices. The solar cells were assembled by placing the platinum electrode (central position) on the WO_3 electrode, and, then, the partially assembled device was finally jointed to the dye-sensitized photoelectrode (working electrode). The platinum layer faced the photoelectrode, and the PEN substrate also faced the WO_3 electrode. The three electrodes were assembled into a sandwich type cell, and 50 μm thick Surlyn hot-melt gasket spaced them in order to create two chambers. The redox electrolyte then filled the space between the electrodes, vacuum pumped through the predrilled hole on the WO_3 electrode. Owing to the holes made in the central electrode (platinum electrode), the electrolyte filled both the chambers. The external holes, used to fill the electrolyte chamber, were sealed using a Surlyn hot-melt film and a cover glass. The redox electrolyte was composed of 0.7 M LiI, 0.005 M I_2, and 0.5 M tert-butylpyridine in dried acetonitrile.

2.5. Optical and Electrochemical Characterization. A Newport AM 1.5 Solar Simulator (Model 91160A equipped with a 300 W xenon arc lamp) served as a light source, and its light intensity (or radiant power) was calibrated to 100 mW/cm² using as reference a Si solar cell. Both open circuit voltage decay (OCVD) and photo-current–voltage measurements were performed using a Keithley unit (Model 2420 Source Meter).

Electrochemical impedance spectroscopy (EIS) spectra have been measured by using an AUTOLAB PGSTAT 100 potentiostat operating in two-electrode mode. Measurements have been carried out in light at open circuit potential conditions: frequency range 100 kHz–10mHz; ac voltage 10 mV. The frequency-dependent impedance

was fitted by using the Z-View software (from Scribner Associates Inc.).

Optical transmittance spectra of the short-circuited devices were observed by a VARIAN 5000 spectrophotometer in a wavelength range between 300 and 2500 nm. Full spectrum measurements were obtained by irradiating the short-circuited device using an array of seven white Luxeon LED (Cool White 6500 K, 7 LED 40 mm−1540 lm at 700 mA), operated by the above-mentioned source meter.

3. RESULTS AND DISCUSSION

3.1. Operating Modes. The proposed architecture consists of three overlapped electrodes: a dye-sensitized titanium dioxide photoelectrode (electrode number 1), a central platinum counter electrode (electrode number 2), and a tungsten oxide electrode (electrode number 3). Figure 2 depicts the possible operation modes of the device:

—Open circuit condition (Figure 2 a): schematic representation of DSSC and PECC circuits. In this case, neither photovoltaic energy nor chromic transition takes place.

—DSSC configuration (Figure 2 b): by connecting the electrodes 1 and 2, the device works as a dye-sensitized solar cell, producing photovoltaic energy when illuminated: the incoming light excites the dye, generating an exciton, split into an electron and a hole. Electrons move toward the external circuit through the mesoporous titania; the holes move through the electrolyte. The I_3^- ion of the redox couple in the

electrolyte reduces the oxidized dye. The platinum carries out a catalytic action, as electrons are transferred to the oxidized electrolyte species. The ion exchange takes place only in the first chamber, between the electrodes 1 and 2. In this circumstance, there is no coloration of the WO_3 electrode (electrode 3).

—PECC configuration (Figure 2 c): the connection of electrodes 1 and 3 generates a photovoltage on the sensitized titania (electrode 1) producing the driving force to inject electrons and inducing the intercalation of Li^+ cations into the tungsten oxide film (electrode 3), resulting in coloration. Once coloration is completed, there is no more electron flow through the PECC circuit because WO_3 is saturated with electrons and Li^+ cations since all the color centers have been occupied by cations, proportionally to the given driving force.

—In this case, the Li^+ ions migration affects both first and second electrolyte chambers: during the coloring processes the cations are attracted by tungsten oxide electrode, negatively charged by the injected electrons. As it is discussed in the following paragraph, during the cations deintercalation (bleaching process), their diffusion depends on the size of the openings made on the central electrode. In this configuration, no photovoltaic energy is produced.

—PVCC configuration (Figure 2 d): by connecting electrode 1 with electrodes 2 and 3, the device produces photovoltaic energy (DSSC circuit—electrodes 1 and 2), and, at the same time, chromic transition takes place (PECC circuit —electrodes 1 and 3). In this condition, tuning the voltage values on the DSSC circuit, it is possible to vary the coloration intensity on the WO_3 electrode. Changing the voltage value means shifting the energy Fermi level of titania, so that the coloration phenomena is produced by the difference of the energy levels between TiO_2 and WO_3.[26] Consequently, it is possible to tune the injected charge on the WO_3 electrode when the relative energy levels of titania and tungsten oxide are modified: if the voltage value is higher than about 0.5—0.6 V, the coloration intensity of WO_3 electrode is high, because the energy Fermi level of titania is higher than the conduction band of the WO_3 electrode. This depends on the fact that the existing energy gap does not allow electrons, intercalated into WO_3 electrode, to flow back to the TiO_2 electrode, through the external PECC circuit; oppositely, if the voltage value is less than 0.5—0.6 V, the Fermi level of titania results lower than that of tungsten oxide and the electrons come back: the coloration intensity is proportional to the voltage applied.

3.2. Photovoltaic and Electrochemical Characterization.

A photovoltaic and electrochemical characterization was performed to assess the impact of the size of platinum electrodes on the photovoltaic and chromic transitions.

IV measurements were carried out to characterize the photovoltaic performances of the devices with respect to the dimensions of three different Pt active areas: 397 mm^2 (sample A), 360 mm^2 (sample B), and 320 mm^2 (sample C). In this order, the photovoltaic conversion efficiencies were 2.75%, 2.35%, and 1.91%, respectively. In Figure 3 we report the curves of the devices in DSSC configuration. A significant dependence of the photovoltaic conversion efficiency on the available platinum surface area was observed: devices embodying a smaller Pt area showed a significant decrease of photovoltaic parameters (Table 1). It is possible to infer that, passing from sample A to sample C, a lower amount of iodine (I_3^-) undergoes reduction, negatively affecting the internal resistance of the cell, especially in terms of fill factor (FF). In sample C
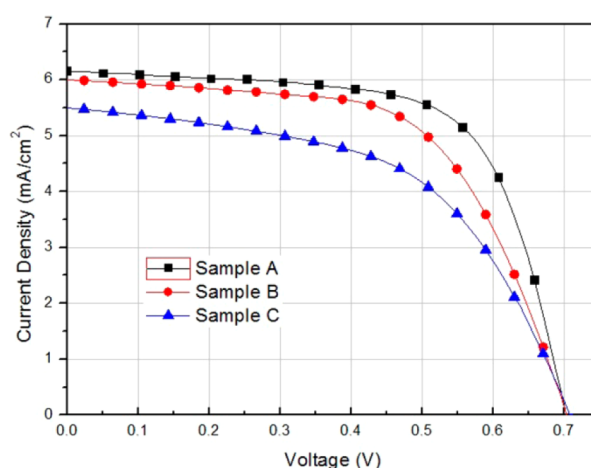

Figure 3. I—V measurements carried out on devices in DSSC configuration. The letters given in the legend refer to a specific active area of the central platinum electrodes.

Table 1. Photovoltaic Parameters Measured in DSSC Mode, Varying the Amount of Active Area of Pt Counter Electrodes[a]

samples	Pt area (mm^2)	η (%)	FF	V_{oc} (V)	Isc (mA/cm^2)
A	397	2.75	0.63	0.70	6.10
B	360	2.35	0.59	0.70	6.02
C	320	1.91	0.54	0.71	5.50

[a]Photovoltaic conversion efficiencies reported in this table showed a standard deviation of 2.5%.

not only the FF but also the current density decreased: this effect may depend on a higher value of charge transfer resistance at the platinum/electrolyte interface. The difference between the performance between samples A and B mainly affected the increase of series resistance (R_{series}); on the other hand, in sample C, a further increase of the R_{series} was added to a significant reduction of the shunt resistance (R_{shunt}), which strongly affects the FF of the PV circuit.[30]

Even if all the samples analyzed have a platinum area bigger than that of the titania photoelectrode (100 mm^2), the progressive reduction of the catalytic surface facing the photoelectrode results in a photovoltaic performance drop.

Table 1 shows the main parameters of the photovoltaic performances of the devices.

As we already demonstrated,[26] a split configuration of the counter electrode does not affect consistently the photovoltaic efficiency of the device in PVCC mode with respect to DSSC mode. Similarly, in this architecture the photovoltaic performances of the devices in PVCC configuration were just 2% lower than those operating in DSSC configuration, due to a small reduction of V_{oc} and FF. In stationary PVCC configuration (when the WO_3 electrode is colored), there is no electrons flow through the PECC circuit. Here the energy produced by the TiO_2 photoanode can be exploited in an external load, and only a small amount (around 2%) is necessary to maintain the WO_3 electrode colored.

EIS measurements were carried out in order to obtain a complete electrochemical assessment for the three-electrode PVCCs. Generally, three characteristic arcs can be obtained from EIS spectra (Nyquist plot, Figure 4) when the device is controlled in open circuit conditions and irradiated with light (100 mW/cm^2). The low-frequency arc (in the mHz) is
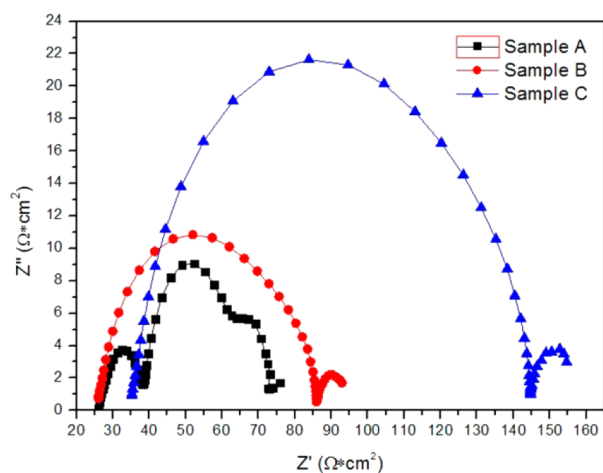
Figure 4. Nyquist plot of the devices varying the platinum active area of the central electrode.

Figure 5. OCVD plot of the device in PVCC configuration varying the platinum active area of the central electrode.

attributed mainly to the Nernst diffusion of I_3^- within the electrolyte. The middle frequency arc (in the $10-100$ Hz region) is related to the transport/recombination process of the injected electrons within the TiO_2 porous films and the charge transfer process of the injected electrons at the interface between TiO_2 and the electrolyte. The high-frequency arc (in the kilohertz range) is related to the charge transfer process at the interface between the redox couple and the platinum counter electrode.[31−34] We made the measurements in open circuit voltage conditions (V_{OC}), in DSSC configuration, to monitor the charge transfer resistance (R_{ct}) at the platinum/electrolyte interface, in devices embodying platinum counter electrodes having different catalytic surface areas.

We mainly observed that passing from sample A to sample C, and then reducing the Pt active area, the R_{ct} parameter increased, producing a significant rising of the series resistance. In more details, in sample A, the R_{ct} was 13.7 ohm/cm^2; in sample B it was 69.8 ohm/cm^2, and in sample C the corresponding value for R_{ct} was 109.6 ohm/cm^2.

The first part of the x-axis, where the Nyquist plot curve intercepts the axis, represents the surface resistance (R_s) of the electrode, which was almost the same for the sample A and B (about 26.5 ohm/cm^2), increasing considerably in sample C where electrodes presented a smaller platinum area up to 35 ohm/cm^2 due to a smaller amount of the PEN-ITO conductive layer.

The open circuit voltage decay (OCVD) measurement gives useful information about the recombination rate between titanium dioxide and the electrolyte in dye-sensitized cells.[34] It consists of measuring the voltage decay of TiO_2 electrode when the lamp is switched off. The recombination rate is proportional to the observed voltage decay. The curves in Figure 5 report the OCVD plot of the devices operating in PVCC mode: the TiO_2 electrode was connected to the Pt electrode, through the potentiostat, and to the WO_3 electrode through an external cable. When irradiated by light and keeping the DSSC circuit in V_{OC} condition, the WO_3 electrode colored via the short-circuited PECC circuit. Once the lamp was switched off, after an initial small and fast voltage decay, due to titanium dioxide electron loss from the conduction band, the voltage decay slowed down as the electrons started to flow back from the PECC circuit with a rate strongly influenced by the lithium diffusion constant in WO_3. The OCVD of TiO_2 in PVCC mode
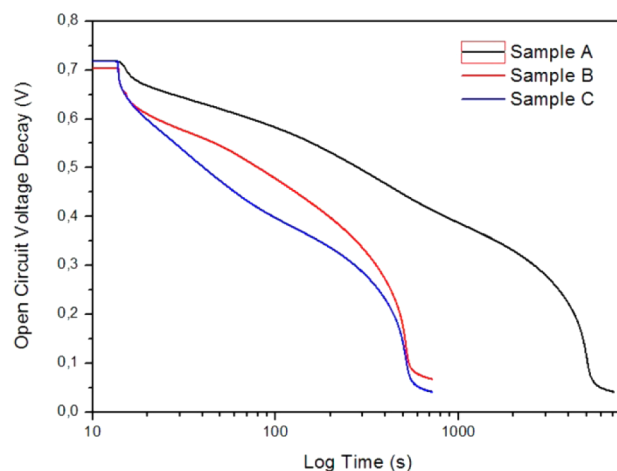
was controlled by the deintercalation of Li^+ ions from WO_3 electrode. For this reason the voltage decay of TiO_2 and the bleaching time of WO_3 are strongly correlated.[26] The faster the deintercalation, the higher the bleaching rate. The time necessary to reach full voltage decay in PVCC configuration coincides with the time required to obtain a complete bleaching of the WO_3 electrode.

As described above and represented in Figure 5, the OCVD plot for devices operating in PVCC mode is reported, varying the hole sizes on the central electrode. We observed that the hole sizes affected the OCVD measurements: for smaller opening sizes, the deintercalation time was higher and the resulting bleaching rate was very slow. On the contrary, in devices embodying counter electrodes having larger openings on the ITO/PEN electrode, the decay time decreased by a significant factor (about 10). At the same time, devices with bigger openings between first and second chambers (samples B and C) showed a completed voltage decay after about 500 s; the one with smaller area (sample A) needed about 5000 s. The reason for this behavior is explained as follows: when the Li^+ ions deintercalate from WO_3, they move toward the TiO_2 diffusing inside the electrolyte with TiO_2 electrode attracting the Li^+ ions during the voltage decay; the shielding effect due to the presence of the central electrode hinders the pathway for cations, producing a high concentration of lithium cations nearby the WO_3 electrode, generating a low gradient. This phenomenon is confirmed by the increase of bleaching time in devices fabricated with smaller communication openings. The intermediate electrode acts as a shield and lowers the deintercalation rate of Li^+ from WO_3.

3.3. Optimization of the Device for Building Integration. In order to enhance the optical transparence of the device, in view of a potential building integration of this smart multifunctional photoelectrochemical windows, we aimed at a further increase of transmittance throughout the visible spectrum. For this reason, a full sensitized organic dye (DYE1) was adopted and embodied in a device having a counter electrode geometry here reported for sample B. In Figure 6, it can be observed that three-electrode PVCCs admit almost all of the visible spectrum through the device, in the transparent state, turning to an opaque state when operating in the PVCC mode.
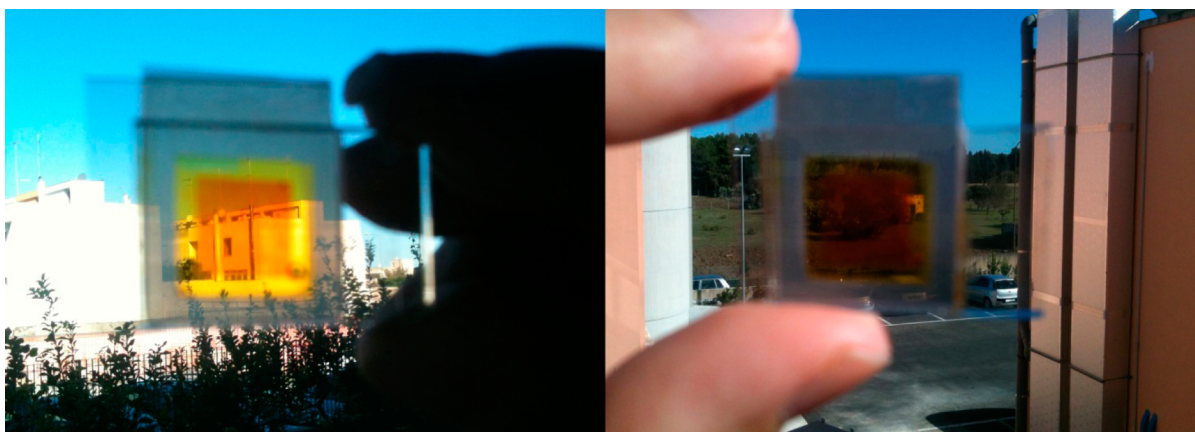
Figure 6. Photos of the device in the transparent and fully colored conditions, respectively. The dye used to optimize the transmittance of the device is DYE1.

In Figure 7, a comparison between the transmittance properties of the devices prepared with N719 and DYE1, in
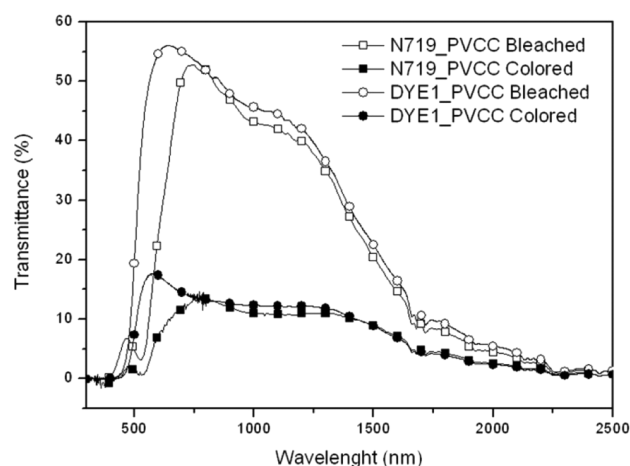

Figure 7. Transmittance spectra of the device, sensitized with N719 and DYE1, respectively, in bleached and colored states.

bleached and colored state, is reported. The measurements were carried out in the conditions described in section 2.5. The spectra with white squares and circles are relative to bleached state; those in the dark refer to colored state. In the bleached state, DYE1-sensitized cell reveals a higher ΔT throughout the visible spectrum (range 400−700 nm) with respect to N719-sensitized devices. Instead, in the infrared part of the spectrum (range 700−2500 nm) the optical transmittance of the dyes is quite similar. Subsequently, to monitor the devices in colored conditions, the PECC circuit (electrodes 1 and 3) was closed. An optical modulation of 40% at 650 nm at 1 sun was observed, starting from $T = 56\%$ in the bleached state. In colored conditions, the DYE1-sensitized device is slightly clearer than the N719-sensitized one. This fact is probably due to the coincident values of the photovoltage and the equal number of color centers in the tungsten oxide films.

Furthermore, the optimized device, embodying DYE1 full sensitized photoelectrodes, with the aim to achieve a high transmittance, provides satisfactory photovoltaic performances ($J_{SC} = 5.10$ mA/cm^2, FF = 0.58, $V_{OC} = 0.68$ V, $\eta = 2.01\%$), if related to the energy conversion efficiency of above-mentioned N719-sensitized PVCCs.

The idea of using a PEN intermediate counter electrode was influenced from several, significant considerations, summarized as follows:

—Fabrication issues: the depth of the electrolyte chamber was reduced due to the use of a thin PEN/ITO layer, replacing a glass one, implying the use of a smaller amount of electrolyte used in the device. Also the distance between photoelectrode and the tungsten oxide counter electrode resulted as reduced.

—Development issues: costs and environmental impacts of such devices could be dramatically cut by simply replacing a typical glass electrode with a polymeric one, especially in view of a potential industrial production.

—Structural issues: the use of a lightweight, interposed PEN layer could imply a significant enhancement in terms of structural performances, prefiguring the fabrication of a laminate glass. Further research activity would be required to demonstrate the latest aspect. The principal challenges to be faced in order to achieve the scale-up of this technologies are those addressed in the fabrication of dye-sensitized solar cells modules.[35]

◼ CONCLUSIONS

The article discloses a novel architecture for PVCCs, based on the design of two distinct counter electrodes consisting of two physically separated platinum and tungsten oxide layers, deposited on different conductive substrates, arranged in order to form two intercommunicating electrolytic chambers. Such an engineered architecture allows a twofold outcome: a self-powered fast-responsive control of the optical transmittance and the generation of electrical power through solar energy conversion. We assessed the electrochemical effect of the different sizes of openings on the intermediate electrode, resulting in different values of available catalytic surface area.

The conversion efficiencies obtained were 2.75%, 2.35%, and 1.91% in samples having different catalytic areas (397, 360, and 320 mm^2, respectively). It has been inferred that the higher the platinum area on the interposed Pt-ITO-PEN counter electrode, the higher the photovoltaic conversion efficiency. Moreover, an increase of platinum surface area generated a slowdown of bleaching processes.

An efficient blue-absorbing organic dye (DYE1) was also tested to optimize the optical transmittance of the device with respect to dye N719. The higher transmittance in the bleached

state of DYE1 fully sensitized devices demonstrates their higher suitability for architectural integration purposes.

In conclusion, this is the first experimental demonstration of a full-area device able to change its transmittance from a highly transparent state to an almost completely dark one. The choice of the electrochromic material and of the dye-sensitization dramatically affects the aesthetic characteristics of the device both in bleached and in colored conditions. This aspect highlights the relevance of chromic engineering, representing a crucial point toward the development of large-area multifunctional smart windows to be integrated in the next generation of building glass facades.

■ AUTHOR INFORMATION

Corresponding Authors
*E-mail: alessandro.cannavale@iit.it.
*E-mail: malara8179@googlemail.com.

Author Contributions
[⊥]These authors equally contributed to the work.

Notes
The authors declare no competing financial interest.

■ ACKNOWLEDGMENTS

■ REFERENCES

(1) Deb, S. K. Opportunities and Challenges in Science and Technology of WO3 for Electrochromic and Related Applications. *Sol. Energy Mater. Sol. Cells* **2008**, *92*, 245−258.

(2) Granqvist, C. G. Oxide Electrochromics: An Introduction to Devices and Materials. *Sol. Energy Mater. Sol. Cells* **2012**, *99*, 1−13.

(3) Jaksic, N. I.; Salahifar, A. Feasibility Study of Electrochromic Windows in Vehicles C. *Sol. Energy Mater. Sol. Cells* **2003**, *79*, 409−423.

(4) Granqvist, C. G.; Lansaker, P. C.; Mlyuka, N. R.; Niklasson, G. A.; Avendano, E. Progress in Chromogenics: New Results for Electrochromic and Thermochromic Materials and Devices. *Sol. Energy Mater. Sol. Cells* **2009**, *93*, 2032−2039.

(5) Tenner, A. D.; Zonneveldt, L. *Proceedings of "The Right Light 5" Conference*, session 11, Nice (France), 2002; pp 279−283.

(6) Cannavale, A.; Fiorito, F.; Resta, D.; Gigli, G. Visual Comfort Assessment of Smart Photovoltachromic Windows. *Energy Build.* **2013**, *65*, 137−145.

(7) Bechinger, C.; Ferrere, S.; Zaban, A.; Sprague, J.; Gregg, B. Photoelectrochromic Windows and Displays. *Nature* **1996**, *383*, 608−610.

(8) Gregg, B. A. Photoelectrochromic Cells and their Applications. *Endeavour* **1997**, *21*, 52−55.

(9) Niklasson, G. A.; Granqvist, C. G. Electrochromics for Smart Windows: Thin Films of Tungsten Oxide and Nickel Oxide, and Devices Based on These. *J. Mater. Chem.* **2007**, *17*, 127−156.

(10) Zheng, H.; Ou, J. Z.; Strano, M. S.; Kaner, R. B.; Mitchell, A.; Kalantar-Zadeh, K. Nanostructured Tungsten Oxide—Properties, Synthesis, and Applications. *Adv. Funct. Mater.* **2011**, *21*, 2175−2196.

(11) Bazilian, M.; Onyeji, I.; Liebreich, M.; MacGill, I.; Chase, J.; Shah, J.; Gielen, D.; Arent, D.; Landfear, D.; Zhengrong, S. Reconsidering the Economics of Photovoltaic Power. *Renewable Energy* **2013**, *53*, 329−338.

(12) He, T.; Yao, J. Photochromic Materials Based on Tungsten Oxide. *J. Mater. Chem.* **2007**, *17*, 4547−4557.

(13) Balaji, S.; Djaoued, Y.; Albert, A. S.; Bruning, R.; Beaudoin, N.; Robichaud, J. Porous Orthorhombic Tungsten Oxide Thin Films: Synthesis, Characterization, and Application in Electrochromic and Photochromic Devices. *J. Mater. Chem.* **2011**, *21*, 3940−3948.

(14) Georg, A.; Opara Krasovec, U. Photoelectrochromic Window with Pt Catalyst. *Thin Solid Films* **2006**, *502*, 246−251.

(15) Hauch, A.; Georg, A.; Baumgartner, S.; Opara Krasovec, U.; Orel, B. New Photoelectrochromic Device. *Electrochim. Acta* **2001**, *46*, 2131−2136.

(16) Leftheriotis, G.; Syrrokostas, G.; Yianoulis, P. Partly Covered Photoelectrochromic Devices with Enhanced Coloration Speed and Efficiency. *Sol. Energy Mater. Sol. Cells* **2012**, *96*, 86−92.

(17) Yang, S.; Zheng, J.; Li, M.; Xu, C. A Novel Photoelectrochromic Device Based on Poly(3,4-(2,2-dimethylpropylenedioxy)thiophene) Thin Film and Dye-Sensitized Solar Cell. *Sol. Energy Mater. Sol. Cells* **2012**, *97*, 186−190.

(18) Hechavarría, L.; Mendoza, N.; Rincon, M. E.; Campos, J.; Hu, H. Photoelectrochromic Performance of Tungsten Oxide Based Devices with PEG−Titanium Complex as Solvent-Free Electrolytes. *Sol. Energy Mater. Sol. Cells* **2012**, *100*, 27−32.

(19) Wua, C.; Hsu, C. Y.; Huang, K.; Nien, P.; Lin, J.; Ho, K. A Photoelectrochromic Device Based on Gel Electrolyte with a Fast Switching Rate. *Sol. Energy Mater. Sol. Cells* **2012**, *99*, 148−153.

(20) Hsu, C.; Lee, K.; Huang, J.; Justin Thomas, K. R.; Lin, J. T.; Ho, K. A Novel Photoelectrochromic Device with Dual Application Based on Poly(3,4-alkylenedioxythiophene) Thin Film and an Organic Dye J. *Power Sources* **2008**, *185*, 1505−1508.

(21) Li, Y.; Hagen, J.; Haarer, D. Novel Photoelectrochromic Cells Containing a Polyaniline Layer and a Dye-Sensitized Nanocrystalline TiO2 Photovoltaic Cell. *Synth. Met.* **1998**, *94*, 273−277.

(22) Huang, L. M.; Kung, C. P.; Hu, C. W.; Peng, C. Y.; Liu, H. C. Tunable Photovoltaic Electrochromic Device and Module. *Sol. Energy Mater. Sol. Cells* **2012**, *107*, 390−395.

(23) Wu, J.; Hsieh, M.; Liao, W.; Wu, W.; Chen, J. Fast-Switching Photovoltachromic Cells with Tunable Transmittance. *ACS Nano* **2009**, *8*, 2297−2303.

(24) O'Regan, B.; Graetzel, M. A Low-Cost, High-Efficiency Solar Cell Based on Dye-Sensitized Colloidal TiO2 Films. *Nature* **1991**, *353*, 737−740.

(25) Cannavale, A.; Manca, M.; Malara, F.; De Marco, L.; Cingolani, R.; Gigli, G. Highly Efficient Smart Photovoltachromic Devices with Tailored Electrolyte Composition. *Energy Environ. Sci.* **2011**, *4*, 2567.

(26) Malara, F.; Cannavale, A.; Gigli, G. Effect of Lithium Intercalation on the Photovoltaic Performances of Photovoltachromic Cells. *Prog. Photovolt.: Res. Appl.* **2013**, DOI: 10.1002/pip.2422.

(27) De Marco, L.; Manca, M.; Giannuzzi, R.; Malara, F.; Melcarne, G.; Ciccarella, G.; Zama, I.; Cingolani, R.; Gigli, G. Novel Preparation Method of TiO2-Nanorod-Based Photoelectrodes for Dye-sensitized Solar Cells with Improved Light-Harvesting Efficiency. *J. Phys. Chem. C* **2010**, *114*, 4228−4236.

(28) De Marco, L.; Manca, M.; Giannuzzi, R.; Belviso, M. R.; Cozzoli, P. D.; Gigli, G. Shape-Tailored TiO2 Nanocrystals with Synergic Peculiarities as Building Blocks for Highly Efficient Multi-Stack Dye Solar Cells. *Energy Environ. Sci.* **2013**, *6*, 1791−1795.

(29) Grisorio, R.; De Marco, L.; Allegretta, G.; Giannuzzi, R.; Suranna, G. P.; Manca, M.; Mastrorilli, P.; Gigli, G. Anchoring Stability and Photovoltaic Properties of new D(-p-A)2 Dyes for Dye-Sensitized Solar Cell Applications. *Dyes Pigm.* **2013**, *98*, 221−231.

(30) Halme, J.; Vahermaa, P.; Miettunen, K.; Lund, P. Device Physics of Dye Solar Cells. *Adv. Mater.* **2010**, *22*, E210−E234.

(31) Fabregat-Santiago, F.; Bisquert, J.; Garcia-Belmonte, G.; Boschloo, G.; Hagfeldt, A. Influence of Electrolyte in Transport and Recombination in Dye-Sensitized Solar Cells Studied by Impedance Spectroscopy. *Sol. Energy Mater. Sol. Cells* **2005**, *87*, 117−131.

(32) Hoshikawa, T.; Yamada, M.; Kikuchi, R.; Eguchi, K. Impedance Analysis of Internal Resistance Affecting the Photoelectrochemical

Performance of Dye-Sensitized Solar Cells. *J. Electrochem. Soc.* **2005**, *152*, E68−E73.

(33) Adachi, M.; Sakamoto, M.; Jiu, J.; Ogata, Y.; Isoda, S. Determination of Parameters of Electron Transport in Dye-Sensitized Solar Cells Using Electrochemical Impedance Spectroscopy. *J. Phys. Chem. B* **2006**, *110*, 13872−13880.

(34) Bisquert, J.; Zaban, A.; Greenshtein, M.; Mora-Seró, I. Determination of Rate Constants for Charge Transfer and the Distribution of Semiconductor and Electrolyte Electronic Energy Levels in Dye-Sensitized Solar Cells by Open-Circuit Photovoltage Decay Method. *J. Am. Chem. Soc.* **2004**, *126*, 13550−13559.

(35) Hinsch, A.; Veurman, W.; Brandt, H.; Loayza Aguirre, R.; Bialecka, K.; Flarup Jensen, K. Worldwide First Fully Up-Scaled Fabrication of 60 × 100 cm^2 Dye Solar Module Prototypes. *Prog. Photovolt.: Res. Appl.* **2012**, *20*, 698−710.